Monthly Notices of the ROYAL ASTRONOMICAL SOCIETY

MNRAS **461,** 1000–1011 (2016) doi:10.1093/mnras/stw1202
Advance Access publication 2016 May 20

A non-local thermodynamical equilibrium line formation for neutral and singly ionized titanium in model atmospheres of reference A–K stars

T. M. Sitnova,[1,2]★ L. I. Mashonkina[1]★ and T. A. Ryabchikova[1]★

[1]*Institute of Astronomy, Russian Academy of Sciences, Pyatnitskaya 48, 119017, Moscow, Russia*
[2]*Sternberg Astronomical Institute; Faculty of Physics, Moscow State University, Universitetsky pr., 13, 119991, Moscow, Russia*

Accepted 2016 May 17. Received 2016 May 13; in original form 2016 March 4

ABSTRACT

We construct a model atom for Ti I–II using more than 3600 measured and predicted energy levels of Ti I and 1800 energy levels of Ti II, and quantum mechanical photoionization cross-sections. Non-local thermodynamical equilibrium (NLTE) line formation for Ti I and Ti II is treated through a wide range of spectral types from A to K, including metal-poor stars with [Fe/H] down to −2.6 dex. NLTE leads to weakened Ti I lines and positive abundance corrections. The magnitude of NLTE corrections is smaller compared to the literature data for FGK atmospheres. NLTE leads to strengthened Ti II lines and negative NLTE abundance corrections. For the first time, we have performed NLTE calculations for Ti I–II in the $6500 \leq T_{\rm eff} \leq 13\,000$ K range. For four A-type stars, we derived in LTE an abundance discrepancy of up to 0.22 dex between Ti I and Ti II, which vanishes in NLTE. For four other A–B stars, with only Ti II lines observed, NLTE leads to a decrease of line-to-line scatter. An efficiency of inelastic Ti I + H I collisions was estimated from an analysis of Ti I and Ti II lines in 17 cool stars with $-2.6 \leq$ [Fe/H] ≤ 0.0. Consistent NLTE abundances from Ti I and Ti II were obtained by applying classical Drawinian rates for the stars with $\log g \geq 4.1$, and neglecting inelastic collisions with H I for the very metal-poor (VMP) giant HD 122563. For the VMP turn-off stars ([Fe/H] ≤ -2 and $\log g \leq 4.1$), we obtained the positive abundance difference Ti I–II already in LTE, which increases in NLTE. Accurate collisional data for Ti I and Ti II are necessary to help solve this problem.

Key words: line: formation – stars: abundances – stars: atmospheres – stars: fundamental parameters.

1 INTRODUCTION

Titanium is observed in lines of two ionization stages, Ti I and Ti II, in a wide range of spectral types from A to K. Experimental oscillator strengths (f_{ij}) for Ti I and Ti II were measured using a common method by Lawler et al. (2013) and Wood et al. (2013), respectively, which permits us to use Ti I and Ti II lines to determine accurate titanium abundances and stellar atmosphere parameters. Bergemann (2011) and Bergemann et al. (2012) investigated the non-local thermodynamic equilibrium (NLTE) line formation for Ti I–II in the atmospheres of cool stars. The first paper presents the NLTE calculations for the Sun and four metal-poor (MP) stars with $T_{\rm eff} \leq 6350$ K, while the second presents those for red supergiants with $3400 \leq T_{\rm eff} \leq 4400$ K, $-0.5 \leq \log g \leq 1.0$ and $-0.5 \leq$ [Fe/H] ≤ 0.5. Bergemann (2011) found that the deviations from LTE are small in the solar atmosphere, with the abundance difference between NLTE and LTE (the NLTE abundance correction, $\Delta_{\rm NLTE}$) not exceeding 0.11 dex for Ti I lines. For the Sun, Bergemann (2011) derived NLTE abundances from Ti I and Ti II lines, consistent within 0.04 dex. However, she failed to achieve the Ti I/Ti II ionization equilibrium for cool MP ($-2.5 \leq$ [Fe/H] ≤ -1.3) dwarfs with well-determined atmospheric parameters. Bergemann (2011) suggested that this can be caused by: (i) neglecting high-excitation levels of Ti I in the used model atom; (ii) using hydrogenic photoionization cross-sections; (iii) using a rough theoretical approximation (Drawin 1968, 1969) for inelastic collisions with hydrogen atoms. We eliminate the first two points in this study. We still rely on the Drawinian approximation because accurate laboratory measurements or quantum mechanical calculations for inelastic Ti I + H I collisions are not available. Poorly known collisions with H I atoms are the main source of the uncertainties in the NLTE results for stars with $T_{\rm eff} \leq 7000$ K.

For the atmospheres hotter than $T_{\rm eff} \geq 6500$ K, the NLTE calculations for Ti I–II have not yet been performed, although the observations indicate a discrepancy in LTE abundances between Ti I

★ E-mail: sitnova@inasan.ru (TMS); lima@inasan.ru (LIM); ryabchik@inasan.ru (TAR)

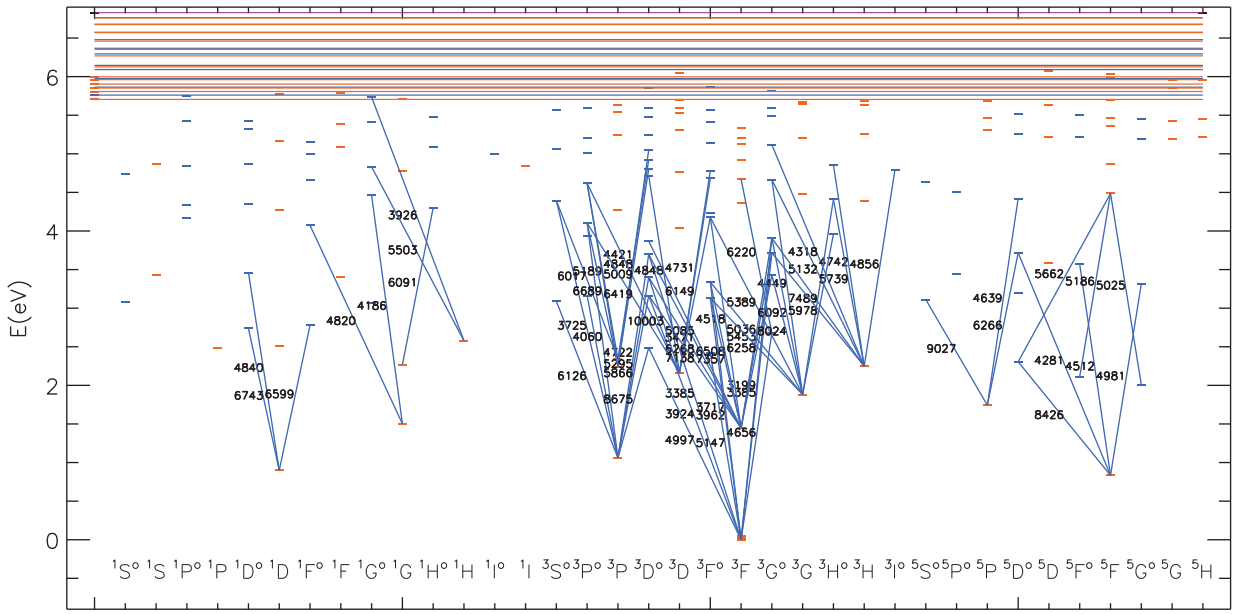

Figure 1. Atomic term structure of Ti I obtained from the laboratory experiments (dashes) and calculations (lines). See text for the sources of data. The spectral lines used in abundance analysis arise in the transitions shown as solid lines. The ionization threshold for Ti I is 6.83 eV.

and Ti II. For example, Bikmaev et al. (2002) derived under the LTE assumption the abundance difference Ti I–Ti II[1] = −0.17 and −0.20 dex for the A-type stars HD 32115 and HD 37954, respectively. Becker (1998) performed the NLTE calculations for Ti II in A-type stars (Vega, supergiants η Leo and 41-3712 from M31) and found that NLTE leads to weakened Ti II lines, with the NLTE abundance corrections being larger for weak lines compared with those calculated for strong lines. Using the model atom from Becker (1998), Przybilla et al. (2006) and Schiller & Przybilla (2008) derived the NLTE abundances from lines of Ti II in BA-type supergiants and concluded that proper NLTE calculations reduce the line-to-line scatter.

We aim to construct a comprehensive model atom of Ti I–II and to treat a reliable method of abundance determination from different lines of Ti I and Ti II in a wide range of stellar spectral types from late B to K, including MP stars. First, we test the new model atom employing the stars with $T_{\rm eff} \geq 7100$ K, where inelastic collisions with hydrogen atoms do not affect the statistical equilibrium (SE). Then, we empirically constrain an efficiency of collisions with H I from analysis of Ti I and Ti II lines in the spectra of cool MP stars. In total, we analyse titanium lines in 25 well-studied stars.

We present the constructed model atom and the NLTE mechanism for Ti I and Ti II in Section 2. In Section 3, we describe observations and stellar parameters of our stellar sample. The obtained results for hot and cool stars are considered in Sections 4 and 5, respectively. Our conclusions and recommendations are given in Section 6.

2 METHOD OF NLTE CALCULATIONS FOR Ti I–II

In this section, we describe the model atom of titanium, the programs used for computing the level populations and spectral-line profiles and the mechanisms of departures from LTE for Ti I and Ti II.

[1] Here, $\log A(X) = \log(N_X/N_{\rm tot})$, where $N_{\rm tot}$ is a total number density and X I–X II means the difference in abundance derived from lines of X I and X II, $\log A$(X I)–$\log A$(X II).

2.1 The model atom

2.1.1 Energy levels

Titanium is almost completely ionized throughout the atmosphere of stars with effective temperatures above 4500 K. For example, the ratio $N_{\rm Ti\,II}/N_{\rm Ti\,I} \simeq 10^2$ throughout the solar atmosphere. Such minority species as Ti I are particularly sensitive to NLTE effects because any small deviation in the intensity of ionizing radiation from the Plank function changes their population greatly. For accurate calculations of the SE, we include in our model atom high-excitation levels of Ti I and Ti II, which establish collisional coupling of Ti I and Ti II levels near the continuum to the ground states of Ti II and Ti III, respectively. Mashonkina et al. (2011) included high-excitation levels of Fe I in their Fe I–II model atom, and found that the SE of iron changed substantially by achieving close collisional coupling of the Fe I levels near the continuum to the ground state of Fe II. Our model atom of titanium (Figs 1 and 2) is constructed using not only all the known energy levels from the National Institute of Standards and Technology (NIST) Atomic Spectra Database (Kramida et al. 2015, using version 3.1.5), but also the predicted levels from the atomic structure calculation of R. Kurucz.[2] The measured levels of Ti I with the excitation energy $E_{\rm exc} \leq 6$ eV belong to 175 terms. Neglecting their fine structure, except for the ground state of Ti I, we obtain 177 levels in the model atom. The predicted and measured levels below the threshold, in total 3500 with $E_{\rm exc} \geq 6$ eV, with common parity and close energies, were combined whenever the energy separation was smaller than $\Delta E = 0.1$ eV. This makes up 17 super-levels.

For Ti II, we use the experimental energy levels belonging to 89 terms with $E_{\rm exc}$ up to 10.5 eV. The fine structure is neglected, except for the ground state of Ti II. The 1800 high-excitation levels with $10.5 \leq E_{\rm exc} \leq 13.6$ eV are used to make up 28 super-levels. The ground state of Ti III completes the system of levels in the model atom.

[2] See http://kurucz.harvard.edu/atoms.html.

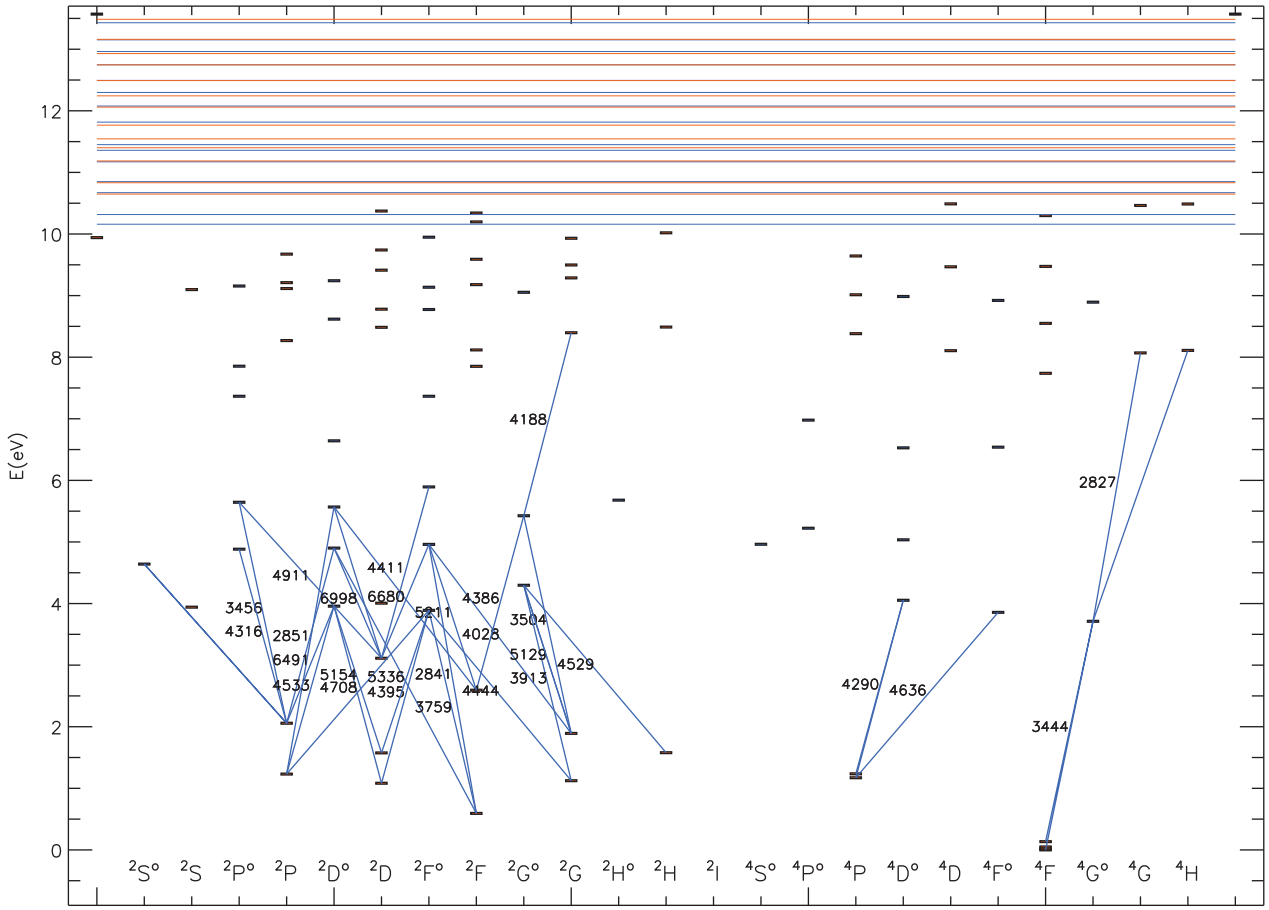

Figure 2. The same as in Fig. 1 for Ti II. The ionization threshold for Ti II is 13.57 eV.

2.1.2 *Radiative bound–bound (b–b) transitions*

In total, 7929 and 3104 allowed transitions of Ti I and Ti II, respectively, occur in our final model atom. Their average *f*-values are calculated using the data from the data base of R. Kurucz. We compared predicted *gf*-values with accurate laboratory data for about 900 transitions of Ti I (Lawler et al. 2013) and found a systematic shift to be minor, with an average difference of $\log gf_{\rm lab} - \log gf_{\rm Kurucz} = -0.05 \pm 0.28$. An advantage of Kurucz's predicted *gf*-values is their completeness, which is extremely important for the SE calculations. For the transitions involving the super-levels, the total *gf*-value was calculated as a sum of *gf* of individual transitions $gf_{\rm tot} = \sum_{i,j}(gf_{i,j})$, $i = 1, \ldots, N_{\rm l}, j = 1, \ldots, N_{\rm u}$, where $N_{\rm l}$ and $N_{\rm u}$ are numbers of individual levels, which form a lower and upper super-level, respectively. Radiative rates were computed using the Voigt profiles for transitions with $f_{ij} \geq 0.10$ and $1800 \leq \lambda \leq 4000$ Å and the Doppler profiles for the remaining ones. The transitions with $f_{ij} \leq 10^{-8}$ were treated as forbidden ones.

2.1.3 *Radiative bound–free (b–f) transitions*

For 115 terms of Ti I with $E_{\rm exc} \leq 5.5$ eV, we use photoionization cross-sections from calculations of Nahar (2015), based on the close-coupling R-matrix method. For 78 terms of Ti II with $E_{\rm exc} \leq 10.0$ eV, we use the data from the quantum mechanical calculations of Keith Butler (private communication). For the remaining high-excitation levels, we assume a hydrogenic approximation with using an effective principle quantum number. We compare the quantum mechanical photoionization cross-sections with the hydrogenic ones for selected levels of Ti I and Ti II in Figs 3 and 4, respectively. For each level, the hydrogenic cross-sections fit, on average, the quantum mechanical ones near the ionization threshold. The difference at frequencies higher than 3.29×10^{15} Hz ($\lambda \leq 912$ Å) weakly affects the photoionization rate because of small flux in this spectral range in the investigated stellar atmospheres.

2.1.4 *Collisional transitions*

All levels in our model atom are coupled via collisional excitation and ionization by electrons and by neutral hydrogen atoms. Our calculations of collisional rates rely on the theoretical approximations because no accurate experimental or theoretical data are available. For electron-impact excitation, we use the formula of van Regemorter (1962) for the allowed transitions and the formula from Woolley & Allen (1948) with a collision strength of 1.0 for the radiatively forbidden transitions. Ionization by electronic collisions is calculated from the Seaton (1962) approximation using the threshold photoionization cross-section.

For collisions with H I atoms, we employ the formula of Steenbock & Holweger (1984) based on the theory of Drawin (1968, 1969) for allowed b–b and b–f transitions and, following Takeda (1994), a simple relation between hydrogen and electron collisional rates, $C_{\rm H} = C_{\rm e}\sqrt{(m_{\rm e}/m_{\rm H})}N_{\rm H}/N_{\rm e}$, for forbidden transitions.

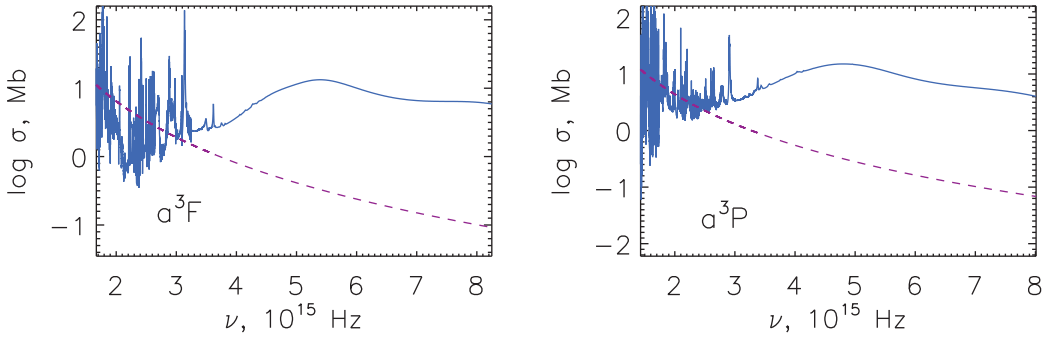

Figure 3. Photoionization cross-sections for the ground state of Ti I (left panel) and the low-excitation level a ^{3}P (right panel) from quantum mechanical calculations (solid curve; Nahar 2015) and computed in the hydrogenic approximation (dashed curve).

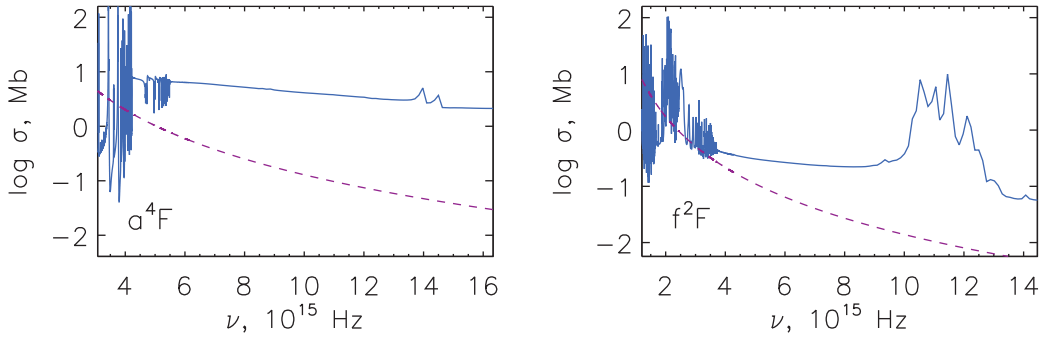

Figure 4. Photoionization cross-sections for the ground state of Ti II (left panel) and the level f ^{2}F (right panel) from quantum mechanical calculations (solid curve; K. Butler) and computed in the hydrogenic approximation (dashed curve).

Because the Drawin formula provides order-of-magnitude estimates, we perform the NLTE calculations using a scaling factor $S_{\rm H} = 0.1$, 0.5 and 1, and we constrain its magnitude empirically from analysis of MP stars.

The nearly resonance charge exchange reaction (CER) $H^+ + Ti\,II \leftrightarrow H\,I + Ti\,III$ takes place because the ionization thresholds for Ti II and H I are 13.57 and 13.60 eV, respectively. There are no data in the literature on cross-sections for this process. In order to inspect an influence of CER on the SE of titanium, we assumed that the analytical fit deduced by Arnaud & Rothenflug (1985) for O I can also be applied to Ti II, because the ionization threshold for O I is close to that for Ti II and amounts to 13.62 eV. Test calculations for A-type stars showed that the CER makes the populations of the ground states of Ti III and Ti II be in thermodynamic equilibrium; nevertheless, no change in the NLTE abundances from lines of Ti II was found. For stars with $T_{\rm eff} \leq 9000$ K, the CER weakly affects the SE because of the small fraction of Ti III.

2.2 Programs and model atmospheres

The coupled radiative transfer and SE equations were solved with a revised version of the DETAIL code by Butler & Giddings (1985). The opacity package of the DETAIL code was updated as described by Przybilla, Nieva & Butler (2011) and Mashonkina et al. (2011), by including the quasi-molecular Lyα satellites following the implementation by Castelli & Kurucz (2001) of the Allard, Kielkopf & Feautrier (1998) theory and using the Opacity Project (see Seaton et al. 1994, for a general review) photoionization cross-sections for the calculations of b–f absorption of C I, N I, O I, Mg I, Si I, Al I, Ca I and Fe I. In addition to the continuous background opacity, the line opacity introduced by H I and metal lines was taken into account by explicitly including it when solving the radiation transfer. The metal line list was extracted from the Kurucz (1994) compilation and the VALD data base (Kupka et al. 1999). The pre-calculated departure coefficients were then used by the SYNTHV_NLTE code updated in Ryabchikova et al. (2016), and based on Tsymbal (1996) to compute the theoretical synthetic spectra. The integration of the SYNTHV_NLTE code in the IDL BINMAG3 code by O. Kochukhov[3] allows us to obtain the best fit to the observed line profiles with the NLTE effects taken into account.

Throughout this study, the element abundance is determined from line profile fitting. For late-type stars, we used classical plane-parallel model atmospheres from the MARCS model grid (Gustafsson et al. 2008), which were interpolated for given $T_{\rm eff}$, log g and [Fe/H] using a FORTRAN-based routine written by Thomas Masseron.[4] For A–B-type stars, the model atmospheres were calculated under the LTE assumption with the code LLMODELS (Shulyak et al. 2004).

For each star, the line list includes unblended lines of various strength ($EW \leq 150$ mÅ, where EW is the line equivalent width) and excitation energies. The full list of the lines is presented in Table 1 along with the transition information, gf-value, excitation energy and damping constants (log $\gamma_{\rm rad}$, log $\gamma_4/N_{\rm e}$, log $\gamma_6/N_{\rm H}$ at 10 000 K). The line list was extracted from the VALD data base (Kupka et al. 1999; Ryabchikova et al. 2015a). The adopted oscillator strengths for most lines of both ions were measured by a common method (Lawler et al. 2013; Wood et al. 2013, Wisconsin data), and, hence, represent a homogeneous set of gf-values.

[3] See http://www.astro.uu.se/~oleg/download.html.
[4] See http://marcs.astro.uu.se/software.php.

Table 1. The list of Ti I and Ti II lines with the adopted atomic data. This table is available in its entirety in a machine-readable form in the online version. A portion is shown here for guidance regarding its form and content.

λ (Å)	E_{exc} (eV)	log *gf*	Transition	log γ_{rad}	log γ_4/N_e	log γ_6/N_H
Ti I						
4008.927	0.021	−1.000	^{3}a ^{3}F–y ^{3}F	8.000	−6.080	−7.750
4060.262	1.052	−0.690	a ^{3}P–x ^{3}P	8.050	−6.050	−7.646
4287.403	0.836	−0.370	a ^{5}F–x ^{5}D	8.230	−6.010	−7.570
4449.143	1.886	0.470	a ^{3}G–v ^{3}G	8.120	−5.560	−7.579
4453.699	1.872	0.100	a ^{3}G–v ^{3}G	8.110	−4.970	−7.582
4512.733	0.836	−0.400	a ^{5}F–y ^{5}F	8.130	−5.120	−7.593
4533.240	0.848	0.540	a ^{5}F–y ^{5}F	8.130	−5.120	−7.593
4534.776	0.836	0.350	a ^{5}F–y ^{5}F	8.130	−5.280	−7.596
4548.763	0.826	−0.280	a ^{5}F–y ^{5}F	8.130	−5.410	−7.598
4555.484	0.848	−0.400	a ^{5}F–y ^{5}F	8.130	−5.280	−7.596
⋮						

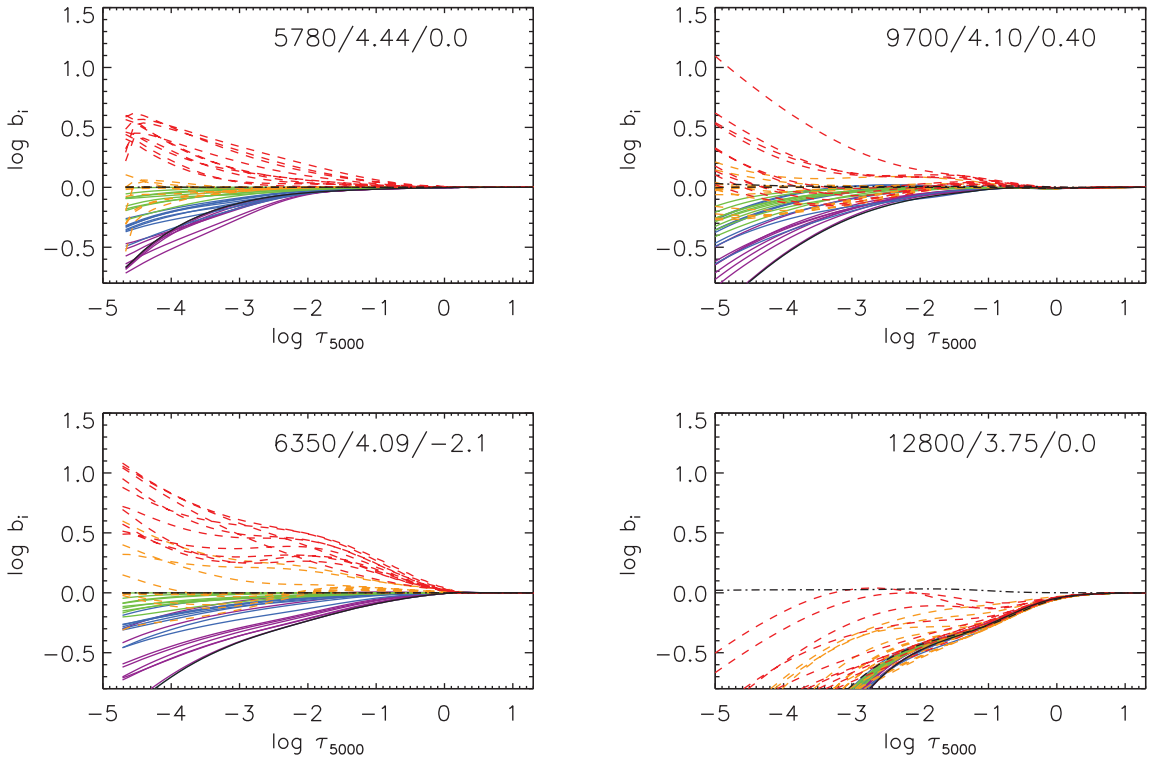

Figure 5. Departure coefficients for the levels of Ti I (solid curves) and Ti II (dotted curves) and the ground state of Ti III (dash-dotted curve) in different model atmospheres. For each model, atmospheric parameters T_{eff}/log *g*/[Fe/H] are indicated.

2.3 Statistical equilibrium of Ti I–II

In this section, we consider the NLTE effects for Ti I–II in various model atmospheres. The deviations from LTE in level populations are characterized by the departure coefficients $b_i = n_i^{NLTE}/n_i^{LTE}$, where n_i^{NLTE} and n_i^{LTE} are the SE and thermal (Saha–Boltzmann) number densities, respectively. The departure coefficients for the selected levels of Ti I, Ti II and the ground state of Ti III in the model atmospheres 5777/4.44/0, 6350/4.09/−2.15, 9700/4.1/0.4 and 12800/3.75/0 are presented in Fig. 5. All the levels retain their LTE populations in deep atmospheric layers below $\log \tau_{5000} = 0$. In the higher atmospheric layers, a total number density of Ti I is lower compared with the TE value. The overionization is caused by superthermal radiation of non-local origin below the thresholds of the low excitation levels of Ti I. In the atmospheres, where Ti II is the majority species, collisional recombinations to the Ti I high-excitation levels followed by cascades of spontaneous transitions tend to compensate for a depopulation of the lower levels of Ti I. However, this process cannot prevent the overionization. High super-levels of Ti I are collisionally coupled to the ground state of Ti II. NLTE leads to weakened lines of Ti I compared to their LTE strengths.

High levels of Ti II are overpopulated via radiative pumping transitions from the low-excitation levels. The NLTE effects for Ti II are small in cool atmospheres. In the models 5780/4.44/0.0 and 6350/4.09/−2.1, a behaviour of the departure coefficients is qualitatively similar. However, a magnitude of the NLTE effects grows towards higher T_{eff} and lower log *g* and [Fe/H]. In the models representing atmospheres of A-type stars, high levels of Ti II retain their LTE populations inward $\log \tau_{5000} = -1.5$, and become

Table 2. Stellar atmosphere parameters and characteristics of the observed spectra. The references cited are as follows: KPNO84, Kurucz et al. (1984); S15, Sitnova et al. (2015); M11, Mashonkina et al. (2011); H93, Hill & Landstreet (1993); F95, Furenlid, Westin & Kurucz (1995); F07, Fossati et al. (2007); F09, Fossati et al. (2009); F10, Fossati et al. (2010); F11, Fossati et al. (2011); L98, Landstreet (1998).

Star	$T_{\rm eff}$ (K)	$\log g$	[Fe/H]	$\xi_{\rm t}$ (km s^{-1})	Ref.	$\lambda/\Delta\lambda$, (10^3)	$S/N >$	Source
Sun	5777	4.44	0.0	0.9	–	300	300	KPNO84
HD 24289	5980	3.71	−1.94	1.1	S15	60	110	S15
HD 64090	5400	4.70	−1.73	0.7	S15	60	280	S15
HD 74000	6225	4.13	−1.97	1.3	S15	60	140	S15
HD 84937	6350	4.09	−2.16	1.7	S15	80	200	UVESPOP[a]
HD 94028	5970	4.33	−1.47	1.3	S15	60	120	S15
HD 103095	5130	4.66	−1.26	0.9	S15	60	200	FOCES[b]
HD 108177	6100	4.22	−1.67	1.1	S15	60	60	S15
HD 140283	5780	3.70	−2.46	1.6	S15	80	200	UVESPOP
BD–4°3208	6390	4.08	−2.20	1.4	S15	80	200	UVESPOP
BD–13°3442	6400	3.95	−2.62	1.4	S15	60	100	S15
BD+7°4841	6130	4.15	−1.46	1.3	S15	120	150	S15
BD+9°0352	6150	4.25	−2.09	1.3	S15	120	160	S15
BD+24°1676	6210	3.90	−2.44	1.5	S15	60	90	S15
BD+29°2091	5860	4.67	−1.91	0.8	S15	60	80	S15
BD+66°0268	5300	4.72	−2.06	0.6	S15	60	110	S15
G 090–003	6010	3.90	−2.04	1.3	S15	60	100	S15
HD 122563	4600	1.60	−2.60	2.0	M11	80	200	UVESPOP
HD 32115	7250	4.20	0.0	2.3	F11	60	490	F11
HD 37594	7150	4.20	−0.30	2.5	F11	60	535	F11
HD 72660	9700	4.10	0.45	1.8	This study	30	150	STIS[c], L98
HD 73666	9380	3.78	0.10	1.8	F07, F10	65	660	F07
HD 145788	9750	3.70	0.0	1.3	F09	115	200	F09
HD 209459 (21 Peg)	10400	3.55	0.0	0.5	F09	120	700	F09
HD 48915 (Sirius)	9850	4.30	0.4	1.8[d]	H93	70	500	F95
HD 17081 (π Cet)	12800	3.75	0.0	1.0	F09	65	200	F09

[a]Bagnulo et al. (2003).
[b]K. Fuhrmann, private communication.
[c]J. Landstreet, private communication.
[d]Sitnova, Mashonkina & Ryabchikova (2013).

underpopulated in the higher atmospheric layers. This results in strengthening the Ti II line cores formed in the uppermost layers compared with LTE. In the hottest model atmosphere 12 800/3.75/0.0, Ti III becomes the majority species, while the levels of Ti II are underpopulated beginning at $\log\tau \simeq 0.5$. Overionization of Ti II results in weakened Ti II lines.

3 OBSERVATIONS AND STELLAR ATMOSPHERE PARAMETERS

Our sample includes the Sun and 24 well-studied stars, which are listed in Table 2. Atmospheric parameters ($T_{\rm eff}$, $\log g$, [Fe/H], $\xi_{\rm t}$) were either determined in our earlier studies or taken from the literature. These parameters were derived by several independent methods, which gave consistent results. Our hot stellar sample consists of A and late B stars, which do not reveal pulsation activity, chemical stratification and magnetic field. For Sirius, π Cet, 21 Peg, HD 32115, HD 37594, HD 73666 and HD 145788, atmospheric parameters were derived by the common method, based on multicolour photometry, analysis of hydrogen Balmer lines and metal lines in high-resolution spectra and comparison of spectrophotometric data with theoretical flux (see Table 2 for the references). For HD 72660, the parameters 9700/4.10/0.45/1.8 were derived by fitting the 4400–5200 and 6400–6700 Å spectral regions with the SME (Spectroscopy Made Easy) program package (Valenti & Piskunov 1996). We used medium-resolution spectrum of HD 72660 extracted from the ELODIE archive (Moultaka et al. 2004).[5] The package SME was tested for Sirius, π Cet, 21 Peg and HD 32115 by Ryabchikova, Piskunov & Shulyak (2015b), who derived practically the same parameters as adopted in the present paper. The atmospheric parameters of HD 72660 agree with the results of Lemke (1989), who derived $T_{\rm eff}/\log g = 9770/4.0$ from photometry and H_β, and of Landstreet et al. (2009), who derived 9650/4.05.

Each cool star of the sample has photometric $T_{\rm eff}$ and $\log g$ based on the *Hipparcos* parallax. We checked in advance whether an ionization equilibrium between Fe I and Fe II is fulfilled in NLTE when using non-spectroscopic parameters. The iron abundances obtained from the lines of Fe I and Fe II in dwarfs agree within 0.05 dex in NLTE, when using $S_{\rm H} = 0.5$ (Sitnova et al. 2015). To confirm the adopted parameters, we checked them with evolutionary tracks and derived reasonable masses and ages. Our sample also includes the most MP giant, HD 122563 ([Fe/H] $= -2.56$), with the accurate *Hipparcos* parallax available. The effective temperature of HD 122563 was determined by Creevey et al. (2012) based on angular diameter measurements.

[5] See http://atlas.obs-hp.fr/elodie/.

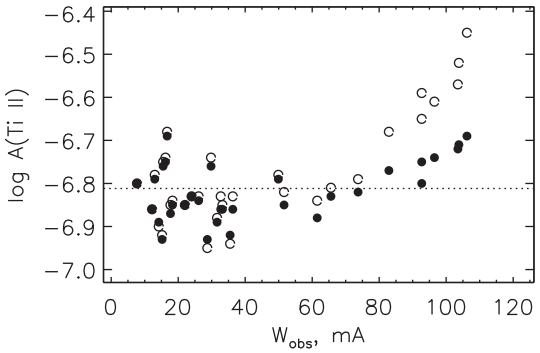

Figure 6. NLTE (filled circles) and LTE (open circles) abundances from the lines of Ti II in HD 145788 as a function of equivalent width.

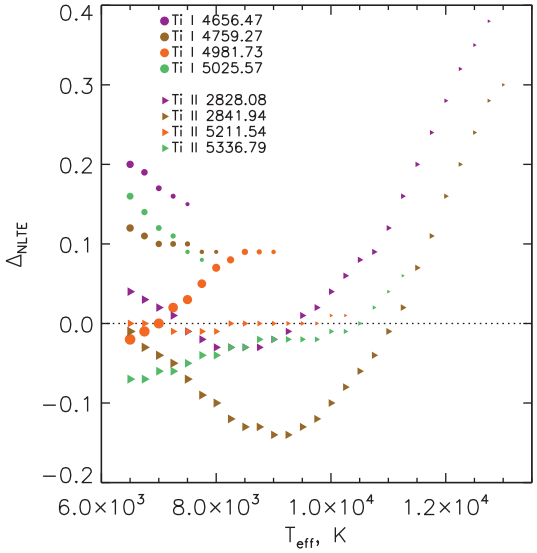

Figure 7. NLTE abundance corrections for the selected lines of Ti I (circles) and Ti II (triangles) shown by different colours. The size of symbol represents an equivalent width of the corresponding line.

4 ANALYSIS OF TI I AND TI II LINES IN A–B-TYPE STARS

A–B-type stars are suitable for testing the treated model atom because the deviations from LTE are large for both Ti I and Ti II and because poorly known inelastic collisions with hydrogen atoms do not affect, or weakly affect, the SE. For example, in the model 7170/4.20/−0.30, the use of $S_H = 0$ and 0.5 leads to a maximal abundance difference of 0.02 and 0.01 dex for individual lines of Ti I and Ti II, respectively.

The lines of two ionization stages are observed in HD 32115, HD 37594, HD 73666 and HD 72660. In the spectra of Sirius, 21 Peg, π Ceti and HD 145788, only the lines of Ti II can be detected. For each star, at least six lines were used to derive the titanium abundance. The LTE and NLTE abundances are given in Table 5. In NLTE, the abundance from Ti I lines increases by 0.05 dex to 0.14 dex for different stars. In contrast, NLTE leads to up to 0.12 dex lower abundance from the lines of Ti II. An exception is the late B star π Cet, where NLTE leads to line weakening and to higher titanium abundance compared with LTE. From the 11 lines of Ti II, we derived $\log A(\mathrm{Ti}) = -7.41 \pm 0.09$ dex and $\log A(\mathrm{Ti}) = -7.14 \pm 0.08$ dex in LTE and NLTE, respectively. Hereafter, the statistical abundance error is the dispersion in the single line measurements, $\sigma = \sqrt{\Sigma(x - x_i)^2/(N-1)}$, where N is the total number of lines used, x is their mean abundance and x_i is the abundance of each individual line. In LTE, for four of our stars, the abundance difference Ti I–Ti II ranges between −0.22 and −0.09 dex, while in NLTE Ti I–Ti II decreases in absolute value and does not exceed 0.07 dex for each of the four stars.

For the A-type stars, the LTE abundances from strong lines of Ti II are higher than those from the weak lines (see Fig. 6 for HD 145788). Such a behaviour can be wrongly interpreted as an underestimation of a microturbulent velocity. For example, to derive consistent LTE abundances from different lines of Ti II in HD 145788, one needs to adopt a microturbulent velocity of $\xi_t = 1.8\,\mathrm{km\,s^{-1}}$, while $\xi_t = 1.3\,\mathrm{km\,s^{-1}}$ was found by Fossati et al. (2009) from lines of Fe II. We show that a discrepancy between strong and weak lines vanishes in NLTE. This is because the strong lines are more affected by NLTE compared with the weak lines. For example, in HD 145788, the cores of the Ti II lines with $EW \sim 100$ mÅ form at the optical depth $\log \tau_{5000} \simeq -2.5$, and their NLTE abundance corrections reach −0.24 dex. For the Ti II lines with $EW \leq 70$ mÅ, the NLTE abundance corrections do not exceed a few hundredths in absolute value. We do not recommend applying the Ti II lines with $EW \geq 70$ mÅ for abundance determination under the LTE assumption. For A–B-type stars, NLTE leads to a significant decrease of line-to-line scatter compared to LTE (Table 5).

We checked the effects of the use of accurate photoionization cross-sections by Nahar (2015) and K. Butler instead of the hydrogenic approximation. The use of quantum mechanical cross-sections for Ti I leads to an increase of the photoionization rates and the deviations from LTE. For example, the NLTE abundance corrections for Ti I lines increase by 0.01–0.02 dex in the model 9700/4.10/0.4/1.8. In the atmospheres with $T_{\rm eff} \leq 10\,500$ K, the NLTE abundances derived from the Ti II lines do not change significantly, when using either accurate or hydrogenic cross-sections. This is because the mechanism of deviations from LTE for Ti II is not ruled by the bound–free transitions. For the hottest star of our sample, HD 17081 (B7 IV), where Ti II is affected by overionization, we found that using the accurate cross-sections leads to weakened NLTE effects for Ti II and 0.06 dex smaller NLTE abundance compared with that calculated with the hydrogenic cross-sections. As we adopt the theoretical approximations to calculate electron collision rates, we perform the test calculations. Test calculations with the model atmosphere 7250/4.20/0.0 show that a hundredfold decrease in electron collision rates results in a 0.05 dex increase in the NLTE abundance from Ti I, and up to 0.06 dex decrease in NLTE abundance from the strongest lines of Ti II with $EW = 150$ mÅ.

Thus, analysis of the titanium lines in the hot stars provides evidence that our NLTE method gives reliable results.

For the 22 lines of Ti I and 82 lines of Ti II, we calculated the NLTE abundance corrections in a grid of model atmospheres with $T_{\rm eff}$ from 6500 to 13 000 K with a step of 250 K, $\log g = 4$, [Fe/H] = 0 and $\xi_t = 2\,\mathrm{km\,s^{-1}}$. For lines of Ti I, the NLTE abundance corrections are positive and vary between 0.0 and 0.20 dex (Fig. 7). For Ti II, the NLTE abundance corrections are negative for $T_{\rm eff} \leq 10\,000$ K and can be up to −0.17 dex. In the atmospheres with $T_{\rm eff} \geq 10\,000$ K, the lines of neutral titanium cannot be detected, and the NLTE abundance corrections for lines of Ti II are positive and reach 0.37 dex. The data are available as online material (Table 3).

Table 3. NLTE abundance corrections and equivalent widths for the lines of Ti I and Ti II depending on $T_{\rm eff}$ in the models with $\log g = 4$, [Fe/H] = 0 and $\xi_{\rm t} = 2\,{\rm km\,s^{-1}}$. This table is available in its entirety in a machine-readable form in the online version. A portion is shown here for guidance regarding its form and content. If $EW = -1$ and $\Delta_{\rm NLTE} = -1$, this means that $EW < 5$ mÅ in a given model atmosphere.

$T_{\rm eff\,1}$ (K)	$T_{\rm eff\,2}$	...	$T_{\rm eff\,26}$	$T_{\rm eff\,27}$
EW_1 (mÅ)	EW_2	...	EW_{26}	EW_{27}
$\Delta_{\rm NLTE\,1}$	$\Delta_{\rm NLTE\,2}$	...	$\Delta_{\rm NLTE\,26}$	$\Delta_{\rm NLTE\,27}$
6500	6750	...	12 750	13 000
...				
5210.3838 Å Ti I $E_{\rm exc} = 0.048$ eV $\log gf = -0.820$				
54	40	...	−1	−1
0.17	0.17	...	−1.00	−1.00
...				
4395.0308 Å Ti II $E_{\rm exc} = 1.084$ eV $\log gf = -0.540$				
176	169	...	15	12
−0.09	−0.10	...	0.25	0.26

Table 4. Abundance difference Ti I–Ti II for cool stars of the sample in different line-formation scenarios.

Star	LTE	NLTE, $S_{\rm H}$		
		1	0.5	0.1
Sun	−0.05	−0.03	−0.02	0.00
HD 64090	−0.04	−0.01	0.00	0.06
HD 84937	0.03	0.15	0.19	0.24
HD 94028	−0.11	−0.05	−0.03	0.05
HD 122563	−0.36	−0.18	−0.13	−0.06
BD+07°4841	−0.06	0.02	0.06	
BD+09°0352	−0.06	0.04	0.08	
HD 140283	−0.05	0.09	0.14	
BD+29°2091	−0.14	−0.09	−0.07	
G 090–003	−0.07	0.05	0.09	
HD 24289	0.00	0.14		
HD 74000	0.01	0.12		
HD 103095	0.06	0.07		
HD 108177	−0.07	0.02		
BD–13°3442	0.09	0.23		
BD–04°3208	0.02	0.15		
BD+24°1676	0.07	0.20		

5 ANALYSIS OF TI I AND TI II LINES IN THE REFERENCE LATE-TYPE STARS

5.1 Ti I and Ti II lines in the solar spectrum

We used 27 Ti I and 12 Ti II lines in the solar flux spectrum (Kurucz et al. 1984) to determine the LTE and NLTE abundances. Under the LTE assumption, we derived $\log A_{\rm Ti\,I} = -7.11 \pm 0.06$ dex and $\log A_{\rm Ti\,II} = -7.06 \pm 0.04$ dex from the lines of Ti I and Ti II, respectively. We calculated the NLTE abundances for $S_{\rm H} = 0$, 0.1, 0.5 and 1.0. Abundances consistent within 0.03 dex from Ti I and Ti II were found in NLTE, independent of the adopted $S_{\rm H}$ value (Table 4). This means that the solar analysis does not help to constrain $S_{\rm H}$. Solar titanium abundance averaged over Ti I and Ti II lines, $\log A = -7.09 \pm 0.06$ dex (NLTE, $S_{\rm H} = 1$), agrees with the meteoritic value, $\log A = -7.11 \pm 0.03$ dex (Lodders, Palme & Gail 2009).

The treated NLTE method was applied before publication to check the Ti I/Ti II ionization equilibrium of 11 stars with $5050 \leq T_{\rm eff} \leq 6600$ K, $3.76 \leq \log g \leq 4.47$ and $-0.48 \leq$ [Fe/H] ≤ 0.24 (Ryabchikova et al. 2016). For HD 49933 (6600/4.0/−0.48), the star with the largest deviations from LTE in the sample, the NLTE calculations provide, consistent within the error bars, the Ti I and Ti II based abundances independent of using either $S_{\rm H} = 0.5$ or 1. For the studied stars, the NLTE abundance difference Ti I–Ti II nowhere exceeds 0.06 dex.

5.2 Ti I and Ti II lines in the metal-poor stars

Metal-poor stars suit better for a calibration of the $S_{\rm H}$ parameter than solar-metallicity stars. This is because the deviations from LTE grow with decreasing [Fe/H] as a result of increasing ultraviolet (UV) flux and decreasing electronic number density. Our sample of cool MP dwarfs includes 15 stars with $-2.6 \leq$ [Fe/H] ≤ -1.3. For all the stars, we determined the titanium abundance under the LTE assumption and in NLTE with $S_{\rm H} = 1.0$, and also with $S_{\rm H} = 0.5$ and 0.1 for a few stars. The abundance differences Ti I–Ti II are listed in Table 4 for various line-formation scenarios and shown in Fig. 9 for LTE and NLTE with $S_{\rm H} = 1.0$. For the seven stars, the NLTE calculations result in abundances from Ti I and Ti II, consistent within the error bars. For example, in HD 94028, Ti I–Ti II = −0.11 dex in LTE, and reduces to −0.05 dex in NLTE ($S_{\rm H} = 1$). For the other eight stars, however, an agreement between Ti I and Ti II is better in LTE compared to that in NLTE. Moreover, for these stars, Ti I–Ti II≥ 0 is obtained already in LTE, and the difference increases in NLTE. For example, in BD −13°3442 we derived the largest discrepancy of 0.23 dex when using NLTE with $S_{\rm H} = 1$, while in LTE Ti I–Ti II = 0.09 dex. All these stars, except HD 103095, are either turn-off (TO) stars with $6200 \leq T_{\rm eff} \leq 6400$ K, $3.9 \leq \log g \leq 4.1$, $-2.6 \leq$ [Fe/H] ≤ -1.9, or very metal-poor (VMP) subgiants with $T_{\rm eff} \geq 5780$ K. Because lower $S_{\rm H}$ leads to larger NLTE effects, we do not perform calculations with $S_{\rm H} \leq 1$ for these stars, except for HD 84937. For the eight dwarfs with negative LTE abundance difference Ti I–Ti II, we performed NLTE calculations with $S_{\rm H} = 0.5$. The minimal difference Ti I–Ti II for the maximal number of stars is achieved, when using $S_{\rm H} = 1$.

5.2.1 HD 122563 (MP giant)

In LTE, we derived an abundance difference of Ti I–Ti II = −0.36 dex, and in NLTE it decreases in absolute value and amounts to Ti I–Ti II = −0.18, −0.13 and −0.06 dex, when using $S_{\rm H} = 1.0$, 0.5 and 0.1, respectively. To achieve an agreement between Ti I and Ti II, the lower $S_{\rm H}$ is required, compared with that for the dwarfs. It is worth noting that a similar conclusion was drawn by Mashonkina et al. (2011) from a line-by-line differential analysis of iron lines in HD 122563 relative to the Sun. Mashonkina et al. (2011) derived an abundance difference of Fe I–Fe II = −0.21 dex in LTE and Fe I–Fe II = −0.18, −0.05 and 0.03 dex in NLTE, when using $S_{\rm H} = 1.0$, 0.1 and 0.0, respectively. However, to achieve the Fe I/Fe II balance for a MP TO star, HD 84937, $S_{\rm H} = 1$ is required. In HD 122563, for both Fe I and Fe II and Ti I and Ti II NLTE leads to a smaller abundance difference between the two ionization stages compared to LTE.

5.3 Comparison with other studies

We have the four stars in common with Bergemann (2011): the Sun, HD 84937, HD140283 and HD 122563. For the common lines of Ti I and Ti II used in the solar analyses, we recalculated abundances derived by Bergemann (2011) using *gf*-values adopted in this study. For the majority lines, the LTE abundance difference between Bergemann (2011) and our data does not exceed 0.03

Table 5. Average NLTE and LTE abundances from Ti I and Ti II lines in the programme stars. For the cool stars, the NLTE abundances were derived using $S_H = 1$.

Star	$N_{\rm Ti\,I}$	$\log A({\rm Ti\,I})_{\rm LTE}$	$\log A({\rm Ti\,I})_{\rm NLTE}$	$N_{\rm Ti\,II}$	$\log A({\rm Ti\,II})_{\rm LTE}$	$\log A({\rm Ti\,II})_{\rm NLTE}$
HD 37594	8	-7.23 ± 0.13	-7.11 ± 0.11	27	-7.01 ± 0.15	-7.04 ± 0.11
HD 32115	6	-7.45 ± 0.05	-7.31 ± 0.05	9	-7.23 ± 0.07	-7.26 ± 0.05
HD 72660	5	-6.63 ± 0.05	-6.57 ± 0.08	36	-6.54 ± 0.12	-6.59 ± 0.08
HD 73666	2	-6.94 ± 0.02	-6.89 ± 0.09	6	-6.72 ± 0.20	-6.84 ± 0.09
HD 145788				32	-6.76 ± 0.15	-6.81 ± 0.07
Sirius				6	-6.84 ± 0.06	-6.89 ± 0.04
21 Peg				46	-7.24 ± 0.05	-7.24 ± 0.04
π Cet				11	-7.41 ± 0.09	-7.14 ± 0.08
Sun	27	-7.11 ± 0.05	-7.09 ± 0.05	12	-7.06 ± 0.04	-7.06 ± 0.04
BD–13°3442	3	-9.25 ± 0.04	-9.09 ± 0.04	15	-9.34 ± 0.06	-9.32 ± 0.06
BD–04°3208	9	-8.90 ± 0.05	-8.77 ± 0.05	17	-8.92 ± 0.06	-8.92 ± 0.05
BD+7°4841	26	-8.24 ± 0.05	-8.17 ± 0.05	34	-8.17 ± 0.06	-8.19 ± 0.05
BD+9°0352	9	-8.87 ± 0.05	-8.78 ± 0.05	22	-8.81 ± 0.05	-8.82 ± 0.04
BD+24°1676	7	-9.12 ± 0.06	-8.98 ± 0.06	16	-9.19 ± 0.06	-9.18 ± 0.06
BD+29°2091	20	-8.76 ± 0.06	-8.72 ± 0.06	24	-8.62 ± 0.08	-8.63 ± 0.07
HD 24289	16	-8.79 ± 0.10	-8.67 ± 0.10	27	-8.79 ± 0.08	-8.81 ± 0.09
HD 64090	35	-8.73 ± 0.07	-8.71 ± 0.07	30	-8.69 ± 0.06	-8.70 ± 0.05
HD 74000	15	-8.78 ± 0.07	-8.68 ± 0.07	26	-8.79 ± 0.08	-8.80 ± 0.08
HD 84937	12	-8.84 ± 0.04	-8.71 ± 0.04	15	-8.87 ± 0.08	-8.86 ± 0.08
HD 94028	26	-8.34 ± 0.06	-8.30 ± 0.07	26	-8.23 ± 0.04	-8.24 ± 0.05
HD 103095	37	-8.06 ± 0.09	-8.05 ± 0.09	29	-8.12 ± 0.07	-8.12 ± 0.07
HD 108177	14	-8.50 ± 0.06	-8.43 ± 0.07	12	-8.43 ± 0.07	-8.45 ± 0.06
HD 122563	22	-9.82 ± 0.07	-9.64 ± 0.08	36	-9.46 ± 0.06	-9.46 ± 0.07
HD 140283	19	-9.36 ± 0.07	-9.21 ± 0.07	25	-9.31 ± 0.05	-9.30 ± 0.05
G 090–03	18	-8.85 ± 0.07	-8.75 ± 0.07	30	-8.78 ± 0.07	-8.79 ± 0.06

dex and nowhere exceeds 0.05 dex. We also compared the NLTE abundance corrections for Ti I. Bergemann (2011) adopted $S_H = 3$ in the NLTE calculations, while we use $S_H = 1$. However, for the majority lines, she computed larger NLTE abundance corrections, by up to 0.03 dex (for Ti I 4981Å). Bergemann (2011) derived with $S_H = 3$ the average abundance difference Ti $_{\rm NLTE}$–Ti $_{\rm LTE}$ = 0.05 dex, while we obtain the same value, when using $S_H = 0.5$. The smaller NLTE effects in this study compared with Bergemann (2011) are due to using a comprehensive model atom that includes predicted high-excitation levels of Ti I.

The difference between our results and the Bergemann (2011) NLTE results grows when moving to the MP stars. We compare the abundance differences Ti $_{\rm NLTE}$–Ti $_{\rm LTE}$ and Ti I-Ti II. For HD 84937, Bergemann (2011) derived Ti $_{\rm NLTE}$–Ti $_{\rm LTE}$ = 0.14 dex using S_H = 3 and the MAFAGS-OS model atmosphere (Grupp, Kurucz & Tan 2009). Using the same stellar parameters for this star, $S_H = 3$, and the MARCS model atmosphere (Gustafsson et al. 2008) we derived Ti $_{\rm NLTE}$–Ti $_{\rm LTE}$ = 0.09 dex. We checked whether this abundance discrepancy can be attributed to different codes for model atmosphere calculation. We calculated Ti I and Ti II abundances with the MARCS and MAFAGS-OS models, and found that the abundance difference does not exceed 0.02 dex for any line. For HD 84937, Bergemann (2011) derived in LTE Ti I–Ti II = 0.11 dex, while we found Ti I–Ti II$_{\rm LTE}$ = 0.03 dex. For HD 140283, she presents abundances calculated only with the MAFAGS-ODF model structure, Ti I–Ti II = 0.02 dex in LTE and 0.16 dex in NLTE ($S_H = 3$). The corresponding values in our calculations are −0.05 dex (LTE) and 0.09 dex (NLTE, $S_H = 1$). A similar situation in our studies was found for HD 122563. We derived discrepancies of Ti I–Ti II=−0.36 and −0.18 dex in LTE and NLTE ($S_H = 1$), respectively. The corresponding LTE and NLTE ($S_H = 3$) values from Bergemann (2011) are −0.40 and −0.10 dex. This abundance comparison indicates that our model atom leads to smaller deviations from LTE compared with those computed by Bergemann (2011).

The star HD 84937 is used as a reference star in many studies, because its atmospheric parameters are well determined by different independent methods. Sneden et al. (2016) investigated the titanium lines under the LTE assumption adopting $T_{\rm eff}$ = 6300 K, $\log g$ = 4.0, [Fe/H] = −2.15, ξ_t = 1.5 km s^{-1} and the interpolated model from Kurucz (2011) model grid. In LTE, they found consistent abundances from Ti I and Ti II. Using the atmospheric parameters adopted in their study and our line list, we derived in LTE Ti I–Ti II = 0.02 dex. A very similar abundance difference of Ti I–Ti II = 0.03 dex was found, with our parameters 6350/4.09/−2.16/1.7. This is because higher $T_{\rm eff}$ and higher $\log g$ lead to a decrease in abundance from Ti I and Ti II, respectively, keeping the ionization balance safe. HD 84937 is one of the stars where NLTE leads to a positive Ti I–Ti II abundance difference, as discussed above.

5.4 What is a source of discrepancy between Ti I and Ti II in VMP TO stars?

5.4.1 Treatment of collisions with H I

The main NLTE mechanism for Ti I is the UV overionization and there is no process that can result in strengthened lines of Ti I and negative NLTE abundance corrections. Inelastic collisions with H I atoms serve as an additional source of thermalization that reduces, but does not cancel, the overionization. It is worth noting that in the atmospheres of our VMP ([Fe/H] ≤ -2) TO stars, the lines of Ti I are weak ($EW \leq 20$ mÅ) and form inwards $\log \tau_{5000} = -1$. The NLTE abundance corrections for Ti II lines are positive in the model 6350/4.09/−2.15, $\Delta_{\rm NLTE} \leq 0.01$ dex when $S_H = 1$, and $\Delta_{\rm NLTE}$ can be up to 0.08 dex, when neglecting collisions with H I atoms. To

what extent inelastic collisions with H I atoms can help to solve the problem of Ti I–Ti II in the MP TO stars will remain unclear until accurate collisional data can be computed for both Ti I + H I and Ti II + H I.

5.4.2 *Uncertainties in* $T_{\rm eff}$

The lines of Ti I are more sensitive to $T_{\rm eff}$ variation compared with Fe I lines, because of the lower ionization threshold for Ti I compared to Fe I. For example, we found an abundance shift of 0.09 dex for Ti I lines, and only 0.05 dex for Fe I, when adopting a $T_{\rm eff}$ 70 K lower for HD 103095 (5130/4.66/−1.26). For this star, a downward revision of $T_{\rm eff}$ by 70 K results in consistent abundances from Ti I and Ti II, and does not destroy Fe I/Fe II ionization equilibrium. However, a different situation was found for the VMP TO stars. For example, we obtained similar abundance shifts of 0.08 and 0.06 dex for Ti I and Fe I, respectively, when adopting $T_{\rm eff}$ 100 K lower for HD 84937 (6350/4.09/−2.16). For this star, the decrease of $T_{\rm eff}$ results in the ionization equilibrium for titanium, but not for iron.

5.4.3 *Three-dimensional effects*

The solution of the NLTE problem with such a comprehensive model atom as treated in this study is only possible, at present, with classical plane-parallel (one-dimensional, 1D) model atmospheres. Neglecting atmospheric inhomogeneities (three-dimensional, 3D, effects) can lead to errors in our results. From hydrodynamical modelling of stellar atmospheres, Collet, Asplund & Trampedach (2007) and Dobrovolskas et al. (2013) predict negative abundance corrections $\Delta_{\rm 3D} = \log A_{\rm 3D} - \log A_{\rm 1D}$ for lines of neutral species in red giant stars. In the models of TO (5900/4.0) stars with [Fe/H] = −2, $\Delta_{\rm 3D}$ increases in absolute value when decreasing the excitation energy of the lower level, and reaches −0.84 and −0.20 dex for the λ = 4000 Å lines with $E_{\rm exc} = 0$ and 2 eV, respectively (Dobrovolskas 2013). All the lines of Ti I used for our MP TO stars have $E_{\rm exc} \leq$ 1.75 eV. The 3D abundance corrections can be either positive or negative, and do not exceed 0.07 dex in absolute value for the lines of Ti II. Negative 3D corrections for Ti I could help to achieve an agreement between Ti I and Ti II. We selected two lines of Ti I, at 4617 Å ($E_{\rm exc}$ = 1.75 eV) and 4681 Å ($E_{\rm exc}$ = 0.05 eV), and Ti II 5336 Å ($E_{\rm exc}$ = 1.58 eV), which give LTE abundances consistent within 0.02 dex, and we calculated the abundance differences Ti I–Ti II for different line-formation scenarios, taking 3D abundance corrections from Dobrovolskas (2013). Abundances from individual lines are shown in Fig. 8. In LTE, we derived Ti I–Ti II = 0.05 dex and −0.49 dex in one and three dimensions, respectively. In NLTE + 3D, we derived −0.27 dex ($S_{\rm H}$ = 1) and −0.16 dex ($S_{\rm H}$ = 0), while Ti I–Ti II = 0.17 dex in NLTE ($S_{\rm H}$ = 1) + 1D, which is our standard scenario. The predicted 3D effects are too strong for low-excitation lines of Ti I and produce a large discrepancy between Ti I lines with different $E_{\rm exc}$, which reaches 0.66 dex in LTE + 3D. We suppose that for MP stars, simply co-adding the NLTE(1D) and 3D(LTE) corrections is too rough a procedure, because both NLTE and 3D effects are equally significant.

5.4.4 *Chromospheres*

One more source can be connected with a star's chromosphere that heats the line-formation layers. An inspiring insight into this problem was presented by Dupree, Avrette & Kurucz (2016). Further efforts should be invested to evaluate a possible influence of the star's chromosphere on the formation of titanium lines.

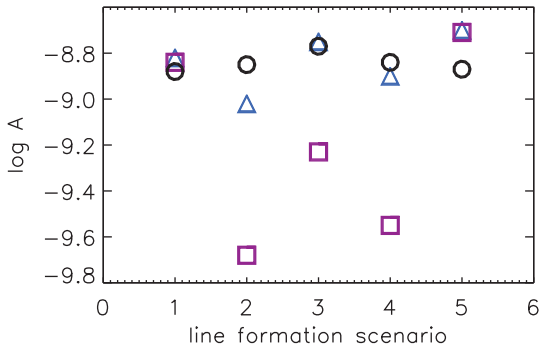

Figure 8. Titanium abundances in HD 84937 from individual lines: Ti I 4617 Å (triangle), Ti I 4681 Å (square), Ti II 5336 Å (circle) in different line-formation scenarios: 1 = LTE+1D; 2 = LTE+3D; 3 = NLTE($S_{\rm H}$ = 0)+3D; 4 = NLTE($S_{\rm H}$ = 1)+3D; 5 = NLTE($S_{\rm H}$ = 1)+1D.

6 CONCLUSIONS

We construct a comprehensive model atom for Ti I–II using the energy levels from laboratory measurements and theoretical predictions and quantum mechanical photoionization cross-sections. NLTE line formation for Ti I and Ti II lines was considered in the 1D LTE model atmospheres of the 25 reference stars with reliable stellar parameters, which cover a broad range of effective temperatures 4600 ≤ $T_{\rm eff}$ ≤ 12 800 K, surface gravities 1.60 ≤ log g ≤ 4.70 and metallicities −2.5 ≤ [Fe/H] ≤ +0.4.

The NLTE calculations for Ti I–II in A-type stars were performed for the first time. The NLTE titanium abundances were determined for the eight stars. For the four stars with both Ti I and Ti II lines observed, NLTE analysis provides abundances from Ti I and Ti II lines, consistent within 0.07 dex, while the corresponding LTE abundance difference can be up to 0.22 dex in absolute value. For each species, NLTE leads to smaller line-to-line scatter compared with LTE. For stars with $T_{\rm eff} \geq$ 7000 K, lines of Ti I and Ti II can be used for atmospheric parameter determination, when taking into account deviations from LTE. For the 22 lines of Ti I and 82 lines of Ti II, we calculated the NLTE abundance corrections in a grid of model atmospheres with $T_{\rm eff}$ from 6500 to 13 000 K, log g = 4, [Fe/H] = 0 and $\xi_{\rm t} = 2\,{\rm km\,s^{-1}}$.

We have made progress in determining the NLTE abundance of titanium for cool stars compared with data from the literature. Taking into account the bulk of the predicted high-excitation levels of Ti I in the model atom, we established close collisional coupling of the Ti I levels near the continuum to the ground state of Ti II, resulting in smaller NLTE effects in cool model atmospheres compared with the Bergemann (2011) data. Because no accurate calculations of inelastic collisions of titanium with neutral hydrogen atoms are available, we use the Drawinian formalism with the scaling factor, which was estimated as $S_{\rm H}$ = 1 from abundance comparison between Ti I and Ti II in the sample of cool main-sequence stars over the wide metallicity range, −2.6 ≤ [Fe/H] ≤ 0.0. For VMP TO stars, NLTE fails to achieve agreement between Ti I and Ti II. Moreover, for these stars we derived positive abundance difference Ti I–Ti II in LTE, which increases in NLTE. To clarify this matter, accurate collisional data for Ti I and Ti II would be extremely helpful.

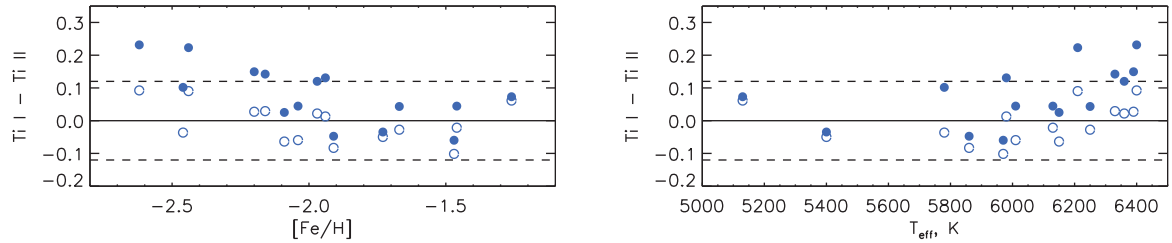

Figure 9. Abundance difference Ti I–Ti II for the 15 cool stars in LTE (open circles) and NLTE with $S_H = 1$ (filled circles). Dashed lines indicate a typical statistical error of $\sqrt{\sigma_{\rm Ti\,I}+\sigma_{\rm Ti\,II}} = \pm 0.12$ dex.

ACKNOWLEDGEMENTS

We thank Keith Butler for computations of the photoionization cross-sections for Ti II. This research was supported by the Russian Foundation for Basic Research (grants 16-32-00695 and 15-02-06046). TS and LM are grateful to the Swiss National Science Foundation (the SCOPES project IZ73Z0–152485). TS and LM are indebted to the International Space Science Institute (ISSI), Bern, Switzerland, for supporting and funding the international team, 'First stars in dwarf galaxies' and 'The Formation and Evolution of the Galactic Halo'. We made use of the NIST, SIMBAD and VALD data bases.

REFERENCES

Allard N. F., Kielkopf J., Feautrier N., 1985, A&A, 330, 782
Arnaud M., Rothenflug R., 1985, A&AS, 60, 425
Bagnulo S., Jehin E., Ledoux C., Cabanac R., Melo C., Gilmozzi R., ESO Paranal Science Operations Team, 2003, The Messenger, 114, 10
Becker S. R., 1998, in Howarth I., ed., ASP Conf. Ser. Vol. 131, Properties of Hot Luminous Stars. Astron. Soc. Pac., San Francisco, p. 137
Bergemann M., 2011, MNRAS, 413, 2184
Bergemann M., Kudritzki R.-P., Plez B., Davies B., Lind K., Gazak Z., 2012, ApJ, 751, 156
Bikmaev I. F. et al., 2002, A&A, 389, 537
Butler K., Giddings J., 1985, Newsletter on the Analysis of Astronomical Spectra, No. 9, University of London
Castelli F., Kurucz R. L., 2001, A&A, 372, 260
Collet R., Asplund M., Trampedach R., 2007, A&A, 469, 687
Creevey O. L. et al., 2012, A&A, 545, A17
Dobrovolskas V., 2013, PhD Dissertation, Vilnius University
Dobrovolskas V., Kučinskas A., Steffen M., Ludwig H.-G., Prakapavičius D., Klevas J., Caffau E., Bonifacio P., 2013, A&A, 559, A102
Drawin H. W., 1969, Z. Physik, 225, 483
Drawin H.-W., 1968, Z. Physik, 211, 404
Dupree A. K., Avrette E. H., Kurucz R. L., 2016, ApJ, 821, L7
Fossati L., Bagnulo S., Monier R., Khan S. A., Kochukhov O., Landstreet J., Wade G., Weiss W., 2007, A&A, 476, 911
Fossati L., Ryabchikova T., Bagnulo S., Alecian E., Grunhut J., Kochukhov O., Wade G., 2009, A&A, 503, 945
Fossati L., Mochnacki S., Landstreet J., Weiss W., 2010, A&A, 510, A8
Fossati L., Ryabchikova T., Shulyak D. V., Haswell C. A., Elmasli A., Pandey C. P., Barnes T. G., Zwintz K., 2011, MNRAS, 417, 495
Furenlid I., Westin T., Kurucz R. L., 1995, in Sauval A. J., Blomme R., Grevesse N., eds, ASP Conf. Ser. Vol. 81, Laboratory and Astronomical High Resolution Spectra. Astron. Soc. Pac., San Francisco, p. 615
Grupp F., Kurucz R. L., Tan K., 2009, A&A, 503, 177
Gustafsson B., Edvardsson B., Eriksson K., Jørgensen U. G., Nordlund Å., Plez B., 2008, A&A, 486, 951
Hill G. M., Landstreet J. D., 1993, A&A, 276, 142
Kramida A., Ralchenko Y., Reader J., NIST ASD Team 2015, NIST Atomic Spectra Database (version 5.3), available at http://physics.nist.gov/asd. National Institute of Standards and Technology, Gaithersburg, MD
Kupka F., Piskunov N., Ryabchikova T. A., Stempels H. C., Weiss W. W., 1999, A&AS, 138, 119
Kurucz R. L., 1994, SYNTHE Spectrum Synthesis Programs and Line Data, CD-ROM No. 18, Cambridge, MA
Kurucz R. L., 2011, Canadian J. Phys., 89, 417
Kurucz R. L., Furenlid I., Brault J., Testerman L., 1984, Solar Flux Atlas from 296 to 1300 nm, National Solar Observatory Atlas, Sunspot. National Solar Observatory, NM
Landstreet J. D., 1998, A&A, 338, 1041
Landstreet J. D., Kupka F., Ford H. A., Officer T., Sigut T. A. A., Silaj J., Strasser S., Townshend A., 2009, A&A, 503, 973
Lawler J. E., Guzman A., Wood M. P., Sneden C., Cowan J. J., 2013, ApJS, 205, 11
Lemke M., 1989, A&A, 225, 125
Lodders K., Palme H., Gail H.-P., 2009, in J. E. Trümper, Landolt-Börnstein – Group VI Astronomy and Astrophysics, Volume 4B. Springer, Berlin, p. 712
Mashonkina L., Gehren T., Shi J.-R., Korn A. J., Grupp F., 2011, A&A, 528, A87
Moultaka J., Ilovaisky S. A., Prugniel P., Soubiran C., 2004, PASP, 116, 693
Nahar S. N., 2015, New Astron., 38, 16
Przybilla N., Butler K., Becker S. R., Kudritzki R. P., 2006, A&A, 445, 1099
Przybilla N., Nieva M.-F., Butler K., 2011, J. Phys. Conf. Ser., 328, 012015
Ryabchikova T., Piskunov N., Kurucz R. L., Stempels H. C., Heiter U., Pakhomov Y., Barklem P. S., 2015a, Phys. Scr., 90, 054005
Ryabchikova T., Piskunov N., Shulyak D., 2015b, in Balega Y. Y., Romanyuk I. I., Kudryavtsev D. O., eds, ASP Conf. Ser. Vol. 494, Physics and Evolution of Magnetic and Related Stars. Astron. Soc. Pac. San Francisco, p. 308
Ryabchikova T. et al., 2016, MNRAS, 456, 1221
Schiller F., Przybilla N., 2008, A&A, 479, 849
Seaton M., 1962, Atomic and Molecular Processes. Academic Press, New York
Seaton M. J., Yan Y., Mihalas D., Pradhan A. K., 1994, MNRAS, 266, 805
Shulyak D., Tsymbal V., Ryabchikova T., Stütz C., Weiss W. W., 2004, A&A, 428, 993
Sitnova T. M., Mashonkina L. I., Ryabchikova T. A., 2013, Astron. Lett., 39, 126
Sitnova T. et al., 2015, ApJ, 808, 148
Sneden C., Cowan J. J., Kobayashi C., Pignatari M., Lawler J. E., Den Hartog E. A., Wood M. P., 2016, ApJ, 817, 53
Steenbock W., Holweger H., 1984, A&A, 130, 319
Takeda Y., 1994, PASJ, 46, 53
Tsymbal V., 1996, in Adelman S. J., Kupka F., Weiss W. W., eds, ASP Conf. Ser. Vol. 108, M.A.S.S., Model Atmospheres and Spectrum Synthesis. Astron. Soc. Pac., San Francisco, p. 198
Valenti J. A., Piskunov N., 1996, A&AS, 118, 595

van Regemorter H., 1962, ApJ, 136, 906
Wood M. P., Lawler J. E., Sneden C., Cowan J. J., 2013, ApJS, 208, 27
Woolley R. v. d. R., Allen C. W., 1948, MNRAS, 108, 292

SUPPORTING INFORMATION

Additional Supporting Information may be found in the online version of this article:

Table 1. The list of Ti I and Ti II lines with the adopted atomic data.
Table 3. NLTE abundance corrections and equivalent widths for the lines of Ti I and Ti II depending on $T_{\rm eff}$ in the models with $\log g = 4$, [Fe/H] $= 0$ and $\xi_{\rm t} = 2\,{\rm km\,s^{-1}}$.

(http://www.mnras.oxfordjournals.org/lookup/suppl/doi:10.1093/mnras/stw1202/-/DC1).

Please note: Oxford University Press is not responsible for the content or functionality of any supporting materials supplied by the authors. Any queries (other than missing material) should be directed to the corresponding author for the article.

This paper has been typeset from a TEX/LATEX file prepared by the author.